Soft and Hard Piezoelectric Ceramics and Single Crystals for Random Vibration Energy Harvesting

Shima Shahab,[a] Sihong Zhao,[b] and Alper Erturk*[b]

Vibration-based energy harvesting for enabling next-generation self-powered devices is a rapidly growing research area. In real-world applications, the ambient vibrational energy is often available in non-deterministic forms rather than the extensively studied deterministic scenarios, such as simple harmonic excitation. It is of interest to choose the best piezoelectric material for a given random excitation. Here, performance comparisons of various soft and hard piezoelectric ceramics and single crystals are presented for electrical power generation under band-limited off-resonance and wideband random vibration energy-harvesting scenarios. For low-frequency off-resonance excitation, it is found that soft piezoelectric ceramics based upon lead zirconate titanate (e.g., PZT-5H and PZT-5A) outperform their hard counterparts (e.g., PZT-4 and PZT-8), and likewise soft single crystals based upon lead magnesium niobate and lead titanate as well as PZT (e.g., PMN-PT and PMN-PZT) outperform the relatively hard ones (e.g., manganese-doped PMN-PZT-Mn). Overall, for such off-resonance random vibrations, PMN-PT is the most suitable choice among the materials studied. For wideband random excitation with a bandwidth covering the fundamental resonance of the harvester, hard piezoelectric ceramics offer larger power output compared to soft ceramics, and likewise hard single crystals produce larger power compared to their soft counterparts. Remarkably, a hard piezoelectric ceramic (e.g., PZT-8) can outperform a soft single crystal (e.g., PMN-PT) for wideband random vibration energy harvesting.

Introduction

The emerging field of vibration-based energy harvesting has been studied extensively by numerous research groups over the past two decades. The goal in this research field is to convert ambient vibrations into electricity and thereby enable self-powered electronic components to minimize the maintenance costs for battery replacement in wireless sensor networks and other wireless devices, as well as to eliminate the chemical waste of conventional batteries. Among the various methods of vibration-to-electric energy conversion,[1] spanning from electromagnetic induction to the use of dielectric elastomers, piezoelectric transduction has been the most heavily researched approach over the past decades.[1–6] The most basic advantages of piezoelectric materials are their ease of application and the mature fabrication techniques[3] available at different geometric scales ranging from macroscale devices to nanowires.

In the existing literature of piezoelectric energy harvesting, linear and nonlinear beams and plates with piezoelectric layers have been the main focus of the mainstream research.[7–19] Numerous articles have reported the development of analytical and numerical electromechanical models of cantilevered energy harvesters for the optimal mechanical and electrical conditions[9,11,20–22] with the assumption that the vibration input to the harvester is of deterministic type, often as simple as harmonic excitation at resonance.[7,12,23,24] However, in most applications, ambient vibrations are manifested in non-deterministic forms. When compared with the amount of published research on piezoelectric energy harvesters with deterministic harmonic input, the existing efforts on piezoelectric energy harvesting from broadband and band-limited random vibrations are very limited.

Other than the early studies by McInnes et al.[25] about exploitation of nonlinear stochastic resonance in energy harvesting and by Scruggs[26] about stochastic control for energy harvesting networks, Halvorsen[27] and Adhikari et al.[28] have presented lumped-parameter (single-degree-of-freedom) models for standard second-order linear vibration energy harvesters under broadband random excitation. They derived closed-form expressions for the harvested power and the optimal electrical loading conditions.[27,28] Based on lumped-parameter modeling, Daqaq[29] and Barton et al.[30] studied electromagnetic energy harvesting using Duffing oscillators under random excitation using analytical and experimental methods. Through similar efforts, Litak et al.[31] and Ali et al.[32] presented numerical simulation and approximate analytical models for broadband random excitation of a bistable piezomagnetoelastic energy harvester.[10] Random excita-

[a] Prof. S. Shahab
Biomedical Engineering and Mechanics Department
Virginia Tech
Blacksburg, VA 24061 (USA)

[b] S. Zhao, Prof. A. Erturk
G. W. Woodruff School of Mechanical Engineering
Georgia Institute of Technology
Atlanta, GA 30332 (USA)
E-mail: alper.erturk@me.gatech.edu

tion of bistable inductive energy harvesting was studied by Daqaq[33] using theoretical methods. Zhao and Erturk[34] accounted for higher vibration modes of the harvester in broadband random excitation using a distributed-parameter electromechanical modeling framework and presented analytical and numerical solutions with experimental validations. In another work,[35] the same authors also explored random excitation of first-order energy harvesters, specifically a piezoelectric stack under compressive axial loading, along with analytical and numerical solutions validated by experiments. Aridogan et al.[36] explored random excitation of a 2D structure (mainly a thin Kirchhoff plate with clamped edges) that hosts multiple structurally integrated piezoelectric patches as energy harvesters.

An overview of thousands of publications in the field of piezoelectric energy harvesting would reveal that the most common piezoelectric energy harvester configuration remains to be a cantilever with piezoelectric laminates undergoing base excitation. How to optimize the geometry and electrical loading conditions for such harvesters has been well studied. In terms of material selection, some researchers explored single-crystal piezoelectric materials due to their larger electromechanical coupling (as compared to that of piezoelectric ceramics, e.g., lead zirconate titanate, PZT), for performance enhancement under harmonic excitation as a simple deterministic excitation form.[37–40] The early work by Erturk et al.[37] on the use of lead magnesium niobate-baed PMN-PZT in a unimorph harvester in bending mode was followed by a shear-mode PMN-PT (PT: lead titanate) harvester by Ren et al.[38] More recently, Yang and Zu[39] and Yang et al.[40] explored PZT-PT and PMN-PT for energy harvesting under harmonic excitation. Although ambient vibrations are often non-deterministic, there has been no effort to guide the choice of the optimal piezoelectric material for energy harvesting from the most typical random excitation scenarios. The current work is an attempt to that end for random-vibration energy-harvesting performance comparison of various piezoelectric ceramics and single crystals. In the following, we consider two types of random excitations of cantilevered bimorph piezoelectric energy harvesters: (1) band-limited low-frequency off-resonance (below the fundamental resonance frequency of the harvester) and (2) wideband (covering the harvester resonance) random excitations. For these excitations, random electrical power generation performance results are analyzed for bimorph energy harvesters made from soft piezoelectric materials PZT-5H and PZT-5A, hard piezoelectric materials PZT-4 and PZT-8, soft piezoelectric single crystals PMN-PT and PMN-PZT, and the relatively hard manganese-doped single crystal PMN-PZT-Mn. First, the approach used in this work is demonstrated using an experimental case study for a PZT-5H cantilevered energy harvester. Band-limited off-resonance and wideband base excitations are demonstrated and the qualitative differences are summarized. After this case study, which also serves as an experimental validation of the approach used herein, random electrical power generation performance comparisons of various piezoelectric ceramics and single crystals are conducted.

The critical material parameters that determine the electrical power generation performance are unveiled for both off-resonance low-frequency and wideband random-vibration energy-harvesting scenarios.

Results and Discussion

Theoretical background

Figure 1 shows the schematic of a cantilevered bimorph piezoelectric energy harvester excited by a dynamic base motion input that represents ambient vibration (in the form of base acceleration $a_B(t)$). The piezoelectric layers are connected in series, as shown in Figure 1; alternatively they
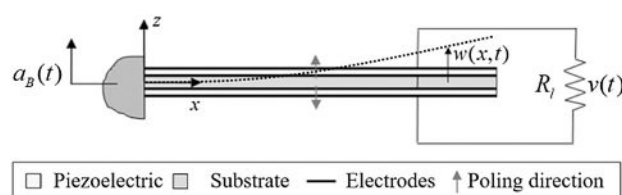

Figure 1. Cantilevered bimorph piezoelectric energy harvester under base excitation: series connection of oppositely poled piezoelectric layers; the resultant terminals are then connected to the electrical load.

could be combined in parallel[5,7] for larger current but lower voltage. The wires from conductive electrodes covering the outer surfaces of the oppositely poled piezoelectric layers are connected to a resistive electrical load (R_l in Figure 1). The typical energy-harvester configuration considered here leverages transverse vibrations of the thin harvester structure for the lowest and most flexible vibrational mode. Therefore, the classical Euler–Bernoulli beam-theory-based energy-harvester formulation is suitable. The analytical model by Erturk and Inman[5,7] is used in this work. The mathematical formulation details for broadband random-vibration energy-harvesting implementation of this model were discussed elsewhere.[34] Briefly, in response to random base acceleration, the two outputs of interest in Figure 1 are the voltage generated across the electrical load, $v(t)$, and the transverse tip vibration response of the cantilever, $w(L,t)$. Unlike the broadband random-vibration energy-harvesting scenario explored previously,[34] which covers the resonance frequencies of the harvester, in many cases, relatively low-frequency random vibrations excite the harvester at off-resonance frequencies. Consequently, in this work, a general band-limited formulation is used and is later employed for comparison of various materials in random power generation.

The expected value of the electrical power output (i.e., the mean electrical power, or the average electrical power) $E[P(t)]$ of the harvester in Figure 1 is

$$E[P(t)] = \int_{-\bar{\omega}}^{\bar{\omega}} \frac{S_0}{R_l}|\alpha(\omega)|^2 d\omega \tag{1}$$

where $\alpha(\omega)$ is the complex frequency response function (FRF) of the harvester that relates the voltage output to base acceleration, S_0 is the power spectral density (PSD) of the base acceleration (ambient vibration input) over the frequency (ω) range of $(0, \bar{\omega}$ (positive side of the PSD), which defines the bandwidth of the ambient vibration energy.

The mean-square tip vibration response of the harvester can be calculated using

$$E[\dot{w}^2(L,t)] = \int_{-\bar{\omega}}^{\bar{\omega}} S_0|\beta(\omega,L)|d\omega \qquad (2)$$

where $\beta(\omega, L)$ is the FRF that relates the transverse tip vibration response of the harvester (in the form of velocity[34] in order to be consistent with LDV measurements in the experiments) to harmonic base acceleration input.

Experimental case study for a PZT-5H bimorph

We demonstrate the approach used in this work and the implementation of the aforementioned electromechanical modeling and analysis framework for a typical cantilevered piezoelectric energy harvester made from PZT-5H, which is a relatively soft piezoelectric ceramic. The experimental setup and the details for the PZT-5H bimorph piezoelectric energy harvester are given in the Experimental Section. The fundamental bending mode resonance frequency of the harvester in short-circuit condition is around 374 Hz (see Figure 12). Therefore, the random base acceleration given in Figure 2a, which has a frequency content roughly up to 300 Hz (Figure 2b), provides a representative off-resonance random excitation scenario for this cantilever. The electromechanical response of the harvester to this excitation is shown in Figure 3 for a 100 kΩ load resistance.
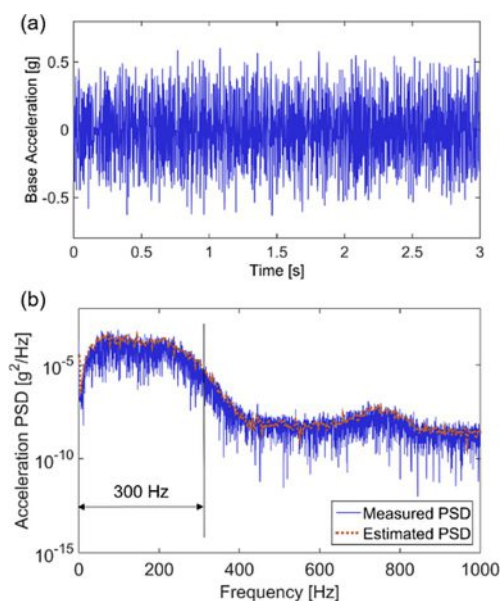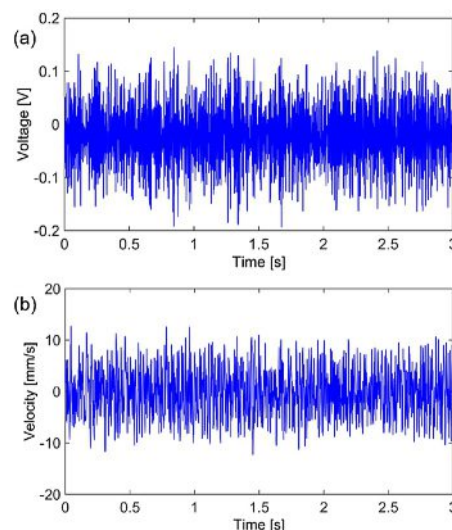

Figure 3. a) Experimental voltage response and b) vibration response of the PZT-5H bimorph energy harvester for a 100 kΩ load resistance across the electrodes for the off-resonance random excitation shown in Figure 2a.

Off-resonance low-frequency random vibration experiments were performed for a broad range of electrical load resistance values. The mean electrical power delivered to the load is shown in Figure 4a. This was calculated based on the analytical voltage FRF (see Figure 12a) using Equation (1). The mean-square vibration response was also simulated based on Equation (2) using the analytical vibration FRF (see Figure 12b) and compared with the experimental data in Figure 4b. The experiments for each resistive load were conducted for five different random time series, as shown. The analytical model predictions and experimental results agree very well for both the electrical and the mechanical responses of the harvester. It is worth noting that because the
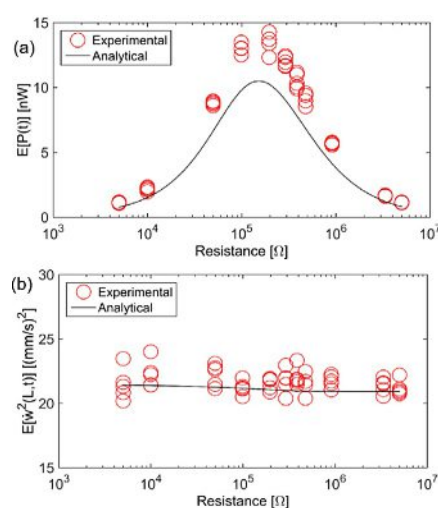

Figure 2. a) Time history of experimental off-resonance random acceleration data with approximately 0–300 Hz bandwidth and b) the PSD.

Figure 4. Model simulation and experimental data for the a) mean electrical power and b) mean-square vibration response of the PZT-5H bimorph energy harvester. Experimental data for each resistive load is obtained for five band-limited (0–300 Hz) off-resonance random time series.

bandwidth of the random vibration does not cover the resonance region, the vibration response is quite insensitive to changing electrical load resistance, i.e., the electrical domain is weakly coupled to the mechanical domain in the off-resonance random excitation scenario.

Recall that the vibration input in Figure 2a was deliberately created below the fundamental resonance frequency of the harvester as a demonstration of off-resonance random excitation and to confirm the ability of the framework to predict the band-limited electromechanical response. Next, random base excitation with a wider bandwidth is considered for the same sample, covering 0–1000 Hz. The excitation in Figure 5a covers the fundamental resonance frequency (around 374 Hz) of the PZT-5H bimorph energy harvester, as can be seen from its PSD (compare Figure 5b with Figure 12). Therefore, in this wide bandwidth case, the resonance response characteristics of the harvester contribute to the response. Figure 6 shows the random voltage response across a 100 kΩ load and the associated vibration response of the harvester at its tip as a function of time.

Experiments were then conducted for the same set of resistive electrical loads as in the previous case to obtain the mean electrical power output and mean-square vibration response as shown in Figure 7. It is not surprising that the maximum power in Figure 7a is much larger (by an order of magnitude) than that in Figure 4a because the bandwidth of the random excitation in Figure 5 covers the resonance of the PZT-5H harvester. Note that there is a qualitative difference between the vibration response of the harvester in Figure 7b, as compared to Figure 4b. Because the resonance behavior is very sensitive to load resistance (Figure 12b inset), in case of wideband random excitation with frequency content covering the resonance, the optimal electrical load resistance that yields the maximum electrical power output cre-
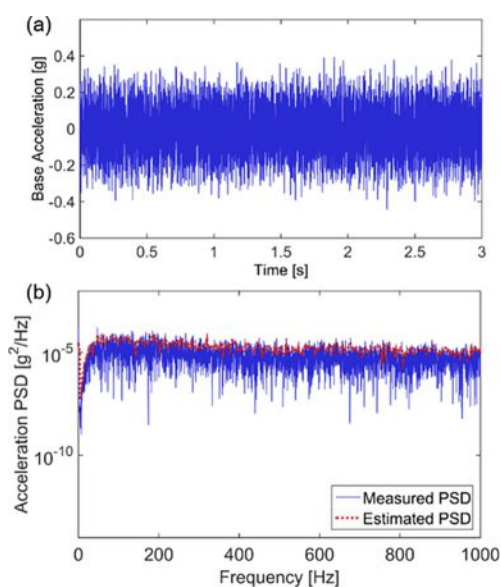

Figure 6. a) Experimental voltage response and b) vibration response of the PZT-5H bimorph energy harvester for a 100 kΩ load resistance across the electrodes for the wideband random excitation shown in Figure 5a.
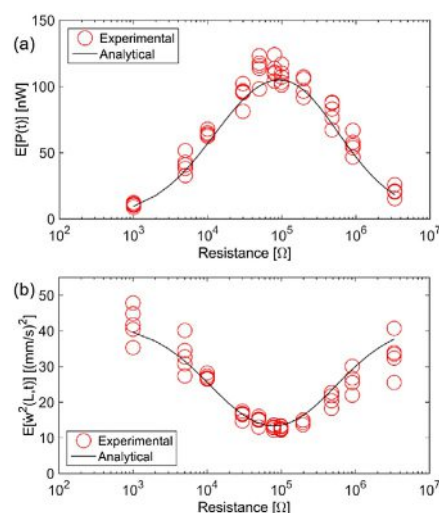
Figure 7. Model simulation and experimental data for the a) mean electrical power and b) mean-square vibration response of the PZT-5H bimorph energy harvester. Experimental data for each resistive load is obtained for five wideband (0–1000 Hz) wideband random time series covering the fundamental resonance frequency of the harvester.

ates significant vibration attenuation in the harvester due to strong coupling.

Results of performance comparison

Having demonstrated the approach for a specific case study on PZT-5H and after experimentally validating the electromechanical framework, we next studied the power generation performance comparison for the following piezoelectric materials: PZT-5H, PZT-5A, PZT-4, PZT-8, PMN-PT, PMN-PZT, and PMN-PZT-Mn. The material properties of the pie-

Figure 5. a) Time history of experimental wideband random acceleration data with approximately 0–1000 Hz bandwidth, covering the fundamental resonance frequency of the harvester and b) the PSD.
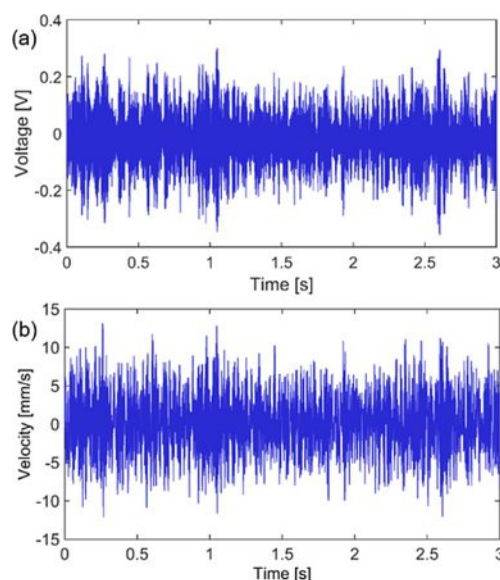
zoelectric ceramics are given in Table 1 and those of the single crystals are shown in Table 2. The properties of PMN-PT (with 33 % PT) are from the article by Cao et al.[41] and those of PMN-PZT and PMN-PZT-Mn are from work by Zhang et al.:[42] the properties of the ceramics PZT-5H, PZT-5A, PZT-4, and PZT-8 are widely available in the relevant literature[5] and on the internet. The last two rows in the table show the relevant electromechanical coupling factor (k_{31}^2) of the respective piezoelectric material as well as the coupling factor weighted by the mechanical quality factor (Q_m).

Table 1. Elastic, piezoelectric, and dielectric properties of the soft and hard piezoelectric ceramics. $\varepsilon_0 = 8.85\ \mathrm{pF\,m^{-1}}$ is the vacuum permittivity.

	PZT-5H	PZT-5A	PZT-4	PZT-8
$d_{31}\ [\mathrm{pm\,V^{-1}}]$	−274	−171	−123	−97
$s_{33}^T\ [\mathrm{pm^2\,N^{-1}}]$	16.5	16.4	12.3	11.5
$\varepsilon_{33}^T/\varepsilon_0$	3400	1700	1300	1000
$\rho\ [\mathrm{kg\,m^{-3}}]$	7500	7750	7500	7600
Q_m	65	75	500	1000
$k_{31}^2 = d_{31}^2/s_{11}^E \varepsilon_{33}^T$	0.151	0.119	0.107	0.0924
$k_{31}^2 Q_m$	9.83	8.89	53.5	92.4

Table 2. Elastic, piezoelectric, and dielectric properties of the soft and hard piezoelectric single crystals.

	PMN-PT	PMN-PZT	PMN-PZT-Mn
$d_{31}\ [\mathrm{pm\,V^{-1}}]$	−1330	−718	−513
$s_{11}^E\ [\mathrm{pm^2\,N^{-1}}]$	69.0	62.0	42.6
$\varepsilon_{33}^T/\varepsilon_0$	8200	4850	3410
$\rho\ [\mathrm{kg\,m^{-3}}]$	8060	7900	7900
Q_m	75	100	1050
$k_{31}^2 = d_{31}^2/s_{11}^E \varepsilon_{33}^T$	0.353	0.194	0.205
$k_{31}^2 Q_m$	26.5	19.4	214.9

PZT-5H, PZT-5A, PZT-4, and PZT-8 are piezoelectric ceramics that are listed in the order from the softest (PZT-5H) to the hardest (PZT-8) ceramics. In simplest terms, a soft piezoelectric ceramic (e.g., PZT-5H) has a larger piezoelectric strain constant (d_{31}) and a smaller mechanical quality factor, whereas a hard piezoelectric ceramic (e.g. PZT-8) offers a smaller piezoelectric constant and a larger mechanical quality factor.

PMN-PT, PMN-PZT, and PMN-PZT-Mn are the single crystal piezoelectric materials explored in this work. In this group, PMN-PT and PMN-PZT are soft single crystals with large piezoelectric strain constants and small mechanical quality factors compared to PMN-PZT-Mn, which is a Mn-modified [42] and relatively hard single crystal in this context.

The goal in this section is to compare the electrical power generation performance results of bimorph energy harvesters made from these materials under band-limited off-resonance random excitation and wideband random excitation cases. The accuracy of the modeling framework used to this end was demonstrated in the previous section for a PZT-5H

energy harvester. The same bimorph dimensions are assumed in this comparison (see Table 3 for the dimensions). For a fair comparison, it was assumed that the entire mechanical loss of each bimorph was due to its mechanical quality factor. Therefore, the dissipative effects of external damping, fabrication (bonding etc.), and clamping were assumed to be identical (and negligible) so that the active materials could be compared under the same conditions by considering their internal mechanical loss only. Therefore, the modal damping ratios were calculated using the quality factors.

First, the analytical FRFs were generated (this is not shown here—similar to Figure 12) for each of the 7 harvesters (for 7 materials) over the frequency range of interest and for a range of load resistance values. Next, the mean electrical power output and mean-square vibration response of each harvester were obtained under off-resonance band-limited and wideband Gaussian random excitations. Because each harvester has a different fundamental resonance frequency, due to the differences between the material properties in Tables 1 and 2—in particular the elastic constants, the frequency bands in the integrals of Equations (1) and (2) were determined as follows: For the off-resonance excitation case, the frequency band covers from quasistatic to half of the fundamental short-circuit resonance frequency for each harvester. For the wideband excitation of each harvester, the frequency bandwidth is from quasistatic to twice the fundamental short-circuit resonance frequency (hence well covering the resonance behavior in the latter case). Figures 8 and 9 summarize the results for band-limited off-resonance
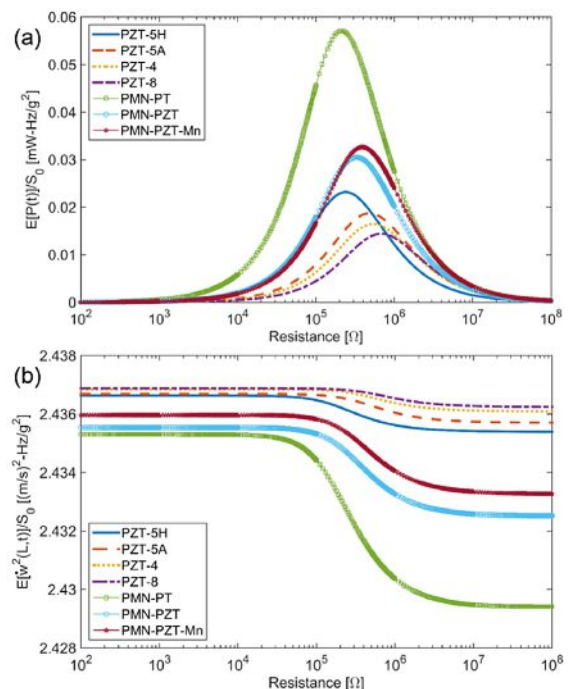

Figure 8. Performance comparison for band-limited off-resonance random excitation of soft and hard piezoelectric ceramics and single crystals: a) mean electrical power and b) mean-square vibration response normalized using the base acceleration PSD. The bandwidth of PSD covers from quasistatic to half of the fundamental resonance frequency of each harvester.
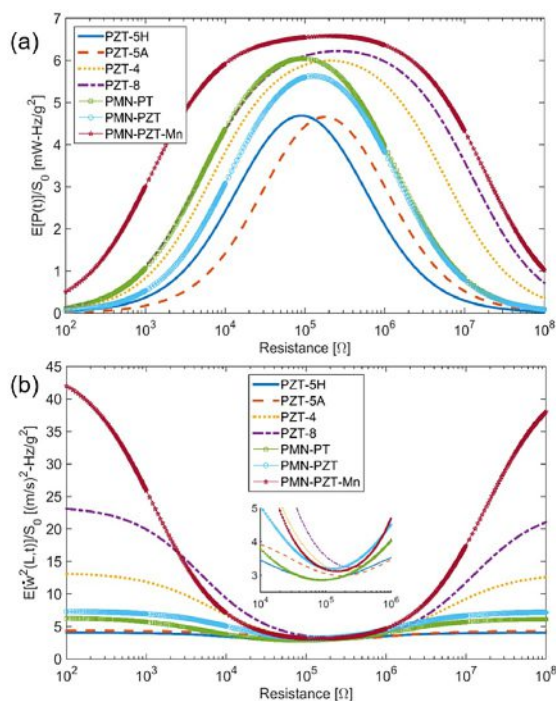
Figure 9. Performance comparison for wideband random excitation of soft and hard piezoelectric ceramics and single crystals, covering the fundamental resonance frequency of each harvester: a) mean electrical power and b) mean-square vibration response normalized by the base acceleration PSD. The bandwidth of PSD covers from quasistatic to twice the fundamental resonance frequency of each harvester.

random excitation and wideband random excitation. Because the system is assumed to be linear, the results (vertical axes) in these figures were normalized by the base acceleration PSD for a comparison.

According to Figure 8a, for low-frequency, off-resonance random excitation, PMN-PT generates the largest power output, and it is followed by PMN-PZT, PMN-PZT-Mn, PZT-5H, PZT-5A, PZT-4, and PZT-8, with the order of the maximum electrical power output. Therefore, it is observed that soft single crystals (e.g., PMN-PT and PMN-PZT) outperform their relatively hard counterparts (in this case only the Mn-doped PMN-PZT, that is, PMN-PZT-Mn[42]). Similarly, soft piezoelectric ceramics (e.g., PZT-5H and PZT-5A) outperform their hard counterparts (e.g., PZT-4 and PZT-8) in terms of power output under off-resonance random excitation. In addition, single crystals outperform ceramics; the maximum power output of PMN-PT bimorph is about 2.5 times larger than that of PZT-5H bimorph.

For relatively wideband random excitation covering the fundamental resonance of each bimorph (see Figure 9a), hard single crystals produce larger power as compared to their soft counterparts (such that PMN-PZT-Mn generates the overall maximum power). Similarly, hard piezoelectric ceramics offer larger power output compared to soft ceramics. Therefore, the order of the piezoelectric materials that produce the maximum power is switched in favor of hard ones such as PMN-PZT-Mn and PZT-8. This is reasonable

because the resonance behavior is covered in the excitation bandwidth and is very sensitive to the amount of dissipation. The materials with higher quality factors (hence lower loss) yield larger power outputs. Furthermore, in Figure 9a, the bimorphs made from hard materials maintain their large response over a broader load resistance. PMN-PZT-Mn has the largest flat region around the optimal resistance, whereas PZT-5H has the narrowest. This characteristic can be useful in applications that involve uncertainty in load resistance. It is particularly important to note that, while the fundamental resonance frequency is covered in the excitation bandwidth for each bimorph, the performance difference between the materials is not by an order of magnitude (unlike the deterministic scenario of harmonic excitation at resonance[5]). Not surprisingly, each of the 7 harvesters is much more efficient for wideband random excitation covering the resonance (when compared to off-resonance), as noted from the two orders of magnitude difference between the power levels in Figures 8a and 9a.

As far as the vibration response of each harvester is concerned, for low-frequency off-resonance excitation, just like the experimental case study for PZT-5H (Figure 4b), the effect of changing load resistance is negligible, as observed from a careful investigation of the vertical axis in Figure 8b. Even for PMN-PT, the vibration response was altered by less than 0.2 % for the electrical load of the maximum power. However, for wideband random excitation covering the resonance frequency (as observed in Figure 7b), the electrical load neighborhood that yields the maximum power output results in significant vibration attenuation in the harvester (Figure 9b). Most notably, PMN-PZT-Mn and PZT-8 yield substantial random vibration attenuation for the optimal electrical load (compared to the short-circuit condition).

The overall results for off-resonance low-frequency random excitation (with a bandwidth that does not cover the fundamental resonance frequency of the harvester) and wideband random excitation (covering the fundamental resonance frequency of the harvester) reveals that the critical parameters are the last two rows in Tables 1 and 2. These respective figures of merit are summarized in Figure 10. When the electromechanical coupling factor values are compared as shown in Figure 10a, the results are in good agreement with the order of the maximum power results in Figure 8a for off-resonance random excitation. Therefore, soft piezoelectric materials, ideally soft single crystals should be preferred for such off-resonance excitation scenarios. On the other hand, a version of the electromechanical coupling factor weighted by the mechanical quality factor, as displayed in Figure 10b, successfully captures the trend in power generation performance results for wideband random excitation in Figure 9a. Therefore, when the random excitation frequency spectrum covers the fundamental resonance frequency of the harvester, the mechanical quality factor becomes critical, and a hard piezoelectric ceramic or single crystal should be preferred, instead of a soft one.
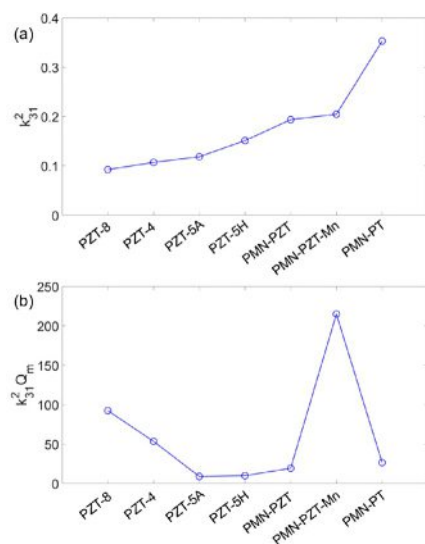
Figure 10. Relevant material parameters to choose the optimal piezoelectric material for two typical random vibration energy harvesting scenarios: a) off-resonance band-limited low-frequency excitation with a bandwidth below the fundamental resonance frequency of the harvester and b) wideband excitation covering the fundamental resonance frequency of the harvester.

Conclusion

The choice of the optimal piezoelectric material in energy harvesting depends on the ambient vibration characteristics. In most cases, the vibration energy that is available to harvest is manifested in non-deterministic forms. This work reports performance comparisons of various soft and hard piezoelectric ceramics and single crystals for electrical power generation under band-limited off-resonance and wideband random-vibration energy-harvesting scenarios. The frequency bandwidth of the former excitation is below the fundamental resonance of the harvester while that of the latter covers the resonance. For these excitations, random electrical power generation performance results were analyzed for bimorph energy harvesters made from soft piezoelectric materials PZT-5H and PZT-5A, hard piezoelectric materials PZT-4 and PZT-8, soft piezoelectric single crystals PMN-PT and PMN-PZT, and the relatively hard (Mn-doped) single crystal PMN-PZT-Mn.

For low-frequency off-resonance excitation of these cantilevered harvesters, soft piezoelectric ceramics (e.g., PZT-5H and PZT-5A) outperform their hard counterparts (e.g., PZT-4 and PZT-8), and similarly soft single crystals (e.g., PMN-PT and PMN-PZT) outperform the relatively hard ones (e.g., Mn-doped PMN-PZT-Mn). For such off-resonance random vibrations, PMN-PT appears to be the most suitable choice among the materials studied. In case of wideband random excitation with a bandwidth covering the fundamental resonance of the harvester, hard piezoelectric ceramics offer larger power output compared to soft ceramics, and likewise hard single crystals produce larger power compared to their soft counterparts. It is noteworthy that unlike the off-resonance scenario, a hard piezoelectric ceramic (e.g., PZT-8)

can easily outperform a soft single crystal (e.g., PMN-PT) for wideband random vibration energy harvesting.

Experimental Section

As shown in Figure 11, a brass-reinforced PZT-5H piezoelectric bimorph (T226-H4-103X by Piezo Systems Inc.) was tested through base excitation experiments for demonstration of the approach used in this work and to validate the electromechanical modeling framework used in the simulation case studies. The bi-
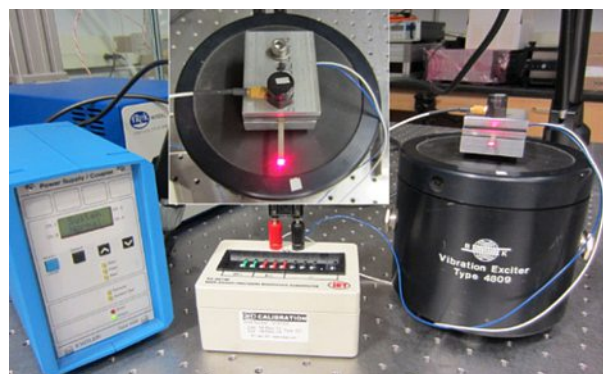

Figure 11. Experimental setup for frequency response function measurements and random vibration tests, and a close-up top view of the PZT-5H energy harvester used for the case study and model validation.

morph cantilever was composed of two PZT-5H layers (with thin nickel electrodes covering the transverse faces) bracketing a brass layer. The geometric and material properties of the PZT-5H bimorph cantilever are listed in Table 3. The electrode leads of the bimorph were connected in series (as depicted in Figure 1) and their resultant was connected to a resistor box. The velocity at the tip of the bimorph was measured by using a Polytec OFV 505 Laser Doppler Vibrometer (LDV) and Polytec OFV-5000 controller. The data in the energy harvesting experiments was analyzed using a Spectral Dynamics SigLab data acquisition device. The data acquisition device received the base acceleration from a Kistler accelerometer after processing through a Kistler signal conditioner. The accelerometer was attached on the top surface of the aluminum clamp and the clamp was mounted onto the armature of an electromechanical shaker (close-up view in Figure 11). The clamp behaved as a rigid body in the frequency range of interest, therefore the accelerometer measured the base acceleration. The excitation was applied to the B&K elec-

Table 3. Geometric and material properties of the PZT-5H bimorph cantilever used in the experimental case study (from Piezo Systems, Inc.).

	Piezoceramic [PZT-5H]	Substrate [brass]
Overhang length [mm]	27.6	27.6
Width [mm]	3.2	3.2
Thickness [mm]	0.258 (each)	0.115
Mass density [kg m^{-3}]	7500	9000
Elastic modulus [GPa]	60.6	105
Piezoelectric constant [C m^{-2}]	−16.6	–
Permittivity constant [nF m^{-1}]	25.55	–

tromechanical shaker through an HP power amplifier/supply for base excitation over a broad range of frequencies.

Experiments were conducted via low-amplitude chirp-type base excitation to obtain the linear electroelastic FRFs of the PZT-5H piezoelectric energy harvester. The voltage and the tip velocity FRFs of the PZT-5H bimorph are shown in Figure 12. The voltage FRF is $|\alpha(\omega)|$ in Equation (1), while the tip velocity FRF is $|\beta(\omega)|$. The tests were conducted for a set of resistors and a broad range of frequencies that cover the first two bending vibration modes. The electrical load resistance values used in the tests ranged from short- to open-circuit conditions of the harvester. The excellent agreement between the experimental results and analytical model validated the electromechanical framework used for modeling the FRFs, which were then used for random vibration analysis via Equations (1) and (2).
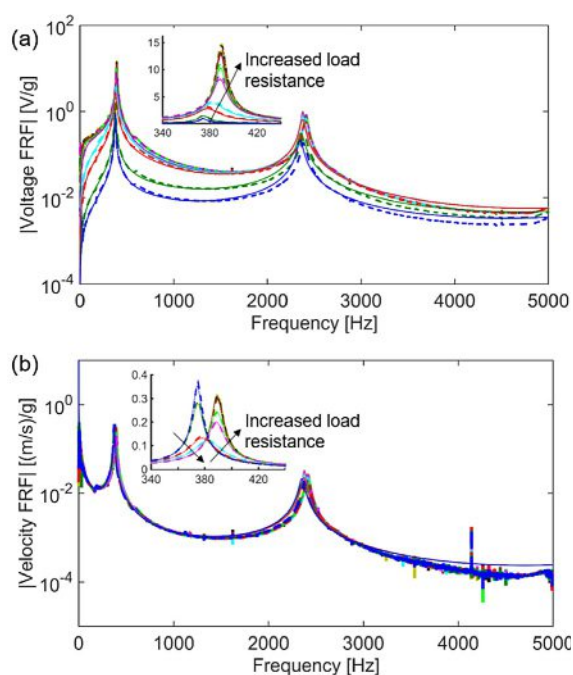

Figure 12. Experimental and analytical electromechanical frequency response functions for a wide range of electrical load resistance values: a) voltage per base acceleration FRFs and b) tip velocity per base acceleration FRFs. Solid lines are model simulations and dashed lines are experimental data.

Conflict of interest

The authors declare no conflict of interest.

[1] *Advances in Energy Harvesting Methods* (Eds.: N. Elvin, A. Erturk), Springer, New York, **2013**.
[2] S. R. Anton, H. A. Sodano, *Smart Mater. Struct.* **2007**, *16*, R1.
[3] K. Cook-Chennault, N. Thambi, A. Sastry, *Smart Mater. Struct.* **2008**, *17*, 043001.
[4] N. S. Hudak, G. G. Amatucci, *J. Appl. Phys.* **2008**, *103*, 101301.
[5] A. Erturk, D. J. Inman, *Piezoelectric Energy Harvesting*, Wiley, Chichester, **2011**.
[6] C. Bowen, H. Kim, P. Weaver, S. Dunn, *Energy Environ. Sci.* **2014**, *7*, 25–44.
[7] A. Erturk, D. J. Inman, *Smart Mater. Struct.* **2009**, *18*, 025009.
[8] F. Cottone, H. Vocca, L. Gammaitoni, *Phys. Rev. Lett.* **2009**, *102*, 080601.
[9] C. J. Rupp, A. Evgrafov, K. Maute, M. L. Dunn, *J. Intell. Mater. Syst. Struct.* **2009**, *20*, 1923–1939.
[10] A. Erturk, J. Hoffmann, D. Inman, *Appl. Phys. Lett.* **2009**, *94*, 254102.
[11] M. I. Friswell, S. Adhikari, *J. Appl. Phys.* **2010**, *108*, 014901.
[12] S. C. Stanton, A. Erturk, B. P. Mann, D. J. Inman, *J. Appl. Phys.* **2010**, *108*, 074903.
[13] S. Zhou, J. Cao, A. Erturk, J. Lin, *Appl. Phys. Lett.* **2013**, *102*, 173901.
[14] S. Leadenham, A. Erturk, *Nonlinear Dyn.* **2015**, *79*, 1727–1743.
[15] U. Aridogan, I. Basdogan, A. Erturk, *Smart Mater. Struct.* **2014**, *23*, 045039.
[16] Z. Yang, Y. Zhu, J. Zu, *Smart Mater. Struct.* **2015**, *24*, 025028.
[17] M. Guan, W.-H. Liao, *Energy Convers. Manage.* **2016**, *111*, 239–244.
[18] S. Zhou, J. Cao, D. J. Inman, J. Lin, S. Liu, Z. Wang, *Appl. Energy* **2014**, *133*, 33–39.
[19] J. Cao, W. Wang, S. Zhou, D. J. Inman, J. Lin, *Appl. Phys. Lett.* **2015**, *107*, 143904.
[20] G. K. Ottman, H. F. Hofmann, G. A. Lesieutre, *IEEE Trans. Power Electronics* **2003**, *18*, 696–703.
[21] Y. Shu, I. Lien, *Smart Mater. Struct.* **2006**, *15*, 1499–1512.
[22] J. M. Renno, M. F. Daqaq, D. J. Inman, *J. Sound Vib.* **2009**, *320*, 386–405.
[23] N. E. Dutoit, B. L. Wardle, S.-G. Kim, *Integr. Ferroelectr.* **2005**, *71*, 121–160.
[24] N. G. Elvin, A. A. Elvin, *J. Intell. Mater. Syst. Struct.* **2009**, *20*, 587–595.
[25] C. McInnes, D. Gorman, M. P. Cartmell, *J. Sound Vib.* **2008**, *318*, 655–662.
[26] J. Scruggs, *J. Sound Vib.* **2009**, *320*, 707–725.
[27] E. Halvorsen, *J. Microelectromech. Syst.* **2008**, *17*, 1061–1071.
[28] S. Adhikari, M. Friswell, D. Inman, *Smart Mater. Struct.* **2009**, *18*, 115005.
[29] M. F. Daqaq, *J. Sound Vib.* **2010**, *329*, 3621–3631.
[30] D. A. Barton, S. G. Burrow, L. R. Clare, *ASME J. Vibr. Acoust.* **2010**, *132*, 021009.
[31] G. Litak, M. Friswell, S. Adhikari, *Appl. Phys. Lett.* **2010**, *96*, 214103.
[32] S. Ali, S. Adhikari, M. Friswell, S. Narayanan, *J. Appl. Phys.* **2011**, *109*, 074904.
[33] M. F. Daqaq, *J. Sound Vib.* **2011**, *330*, 2554–2564.
[34] S. Zhao, A. Erturk, *Smart Mater. Struct.* **2013**, *22*, 015002.
[35] S. Zhao, A. Erturk, *Sens. Actuators A* **2014**, *214*, 58–65.
[36] U. Aridogan, I. Basdogan, A. Erturk, *J. Intell. Mater. Syst. Struct.* **2016**, *27*, 2744–2756.
[37] A. Erturk, O. Bilgen, D. Inman, *Appl. Phys. Lett.* **2008**, *93*, 224102.
[38] B. Ren, S. W. Or, Y. Zhang, Q. Zhang, X. Li, J. Jiao, W. Wang, D. A. Liu, X. Zhao, H. Luo, *Appl. Phys. Lett.* **2010**, *96*, 083502.
[39] Z. Yang, J. Zu, *Energy Convers. Manage.* **2016**, *122*, 321–329.
[40] Z. Yang, Z. Qin, J. Zu, *Sens. Actuators A* **2017**, *266*, 76–84.
[41] H. Cao, V. H. Schmidt, R. Zhang, W. Cao, H. Luo, *J. Appl. Phys.* **2004**, *96*, 549–554.
[42] S. Zhang, S.-M. Lee, D.-H. Kim, H.-Y. Lee, T. R. Shrout, *Appl. Phys. Lett.* **2008**, *93*, 122908.